IEEE Access
Multidisciplinary | Rapid Review | Open Access Journal

Received June 17, 2021, accepted June 30, 2021, date of publication July 5, 2021, date of current version July 13, 2021.

Digital Object Identifier 10.1109/ACCESS.2021.3094470

Electromagnetic Wave Propagation From Low-Earth Orbit Satellite to Ground Station Considering Interpolated Atmospheric Environments

CHANGSEONG KIM[1], (Student Member, IEEE), DONG-YEOP NA[2], (Member, IEEE), AND YONG BAE PARK[1,3], (Senior Member, IEEE)

[1]Department of AI Convergence Network, Ajou University, Gyeonggi-do 16499, South Korea
[2]School of Electrical and Computer Engineering, Purdue University, West Lafayette, IN 47907, USA
[3]Department of Electrical and Computer Engineering, Ajou University, Gyeonggi-do 16499, South Korea

Corresponding author: Yong Bae Park (yong@ajou.ac.kr)

This work was supported by the Ministry of Science and ICT (MSIT), South Korea, under the Information Technology Research Center (ITRC) Support Program supervised by the Institute for Information and Communications Technology Promotion (IITP) under Grant IITP-2020-2018-0-01424.

ABSTRACT We propose a novel method to calculate the electromagnetic (EM) wave propagation from low-earth orbit satellite (LEO) to a ground station based on the physical optics (PO), ray tracing technique, and geometric optics (GO) considering interpolated atmospheric environments. Our method includes the reflector antenna analysis using PO, the interpolation of the meteorological data using PCHIP and Kriging interpolation, transmission analysis using ray tracing and geometrical optics. Tropospheric and stratospheric environments are modeled using meteorological data—air pressure and temperature, relative humidity, and rain rate—measured at 9 different radiosonde observatories in and around South Korea. Furthermore, we utilize Piecewise Cubic Hermite Interpolating Polynomial (PCHIP) and Kriging-exponential methods for vertical and horizontal interpolations of the raw meteorological data, respectively. Hence, the interpolated atmospheric environments are amenable to the best use of ray tracing technique and GO. Subsequently, effective refractive indices of the stratified media can be extracted via millimeter-propagation-model93. The simplified Appleton-Hartree equation characterizes the ionospheric environment. Considering a sun-synchronous orbit satellite passing through South Korea, we calculate atmospheric attenuation, boresight error, received power, and compensation angle of satellite antenna for various conditions.

INDEX TERMS Electromagnetic wave propagation, low-earth orbit satellite, atmospheric environments, ray tracing technique, piecewise cubic Hermite interpolating polynomial.

I. INTRODUCTION

Low-earth orbit (LEO) satellites [1]–[4], revolving at an altitude between 160 to 2,000 km, can offer faster communications with low latency and higher bandwidth at low cost. In addition, a constellation of LEO satellites—Starlink, LeoSat, Boeing, CYGNSS, and Telesat LEO which provide various satellite services such as remote sensing, weather monitoring, internet of things (IoT), and satellite navigation [5], [6]—can attain continuous and global coverage for various communication systems. Especially, a sun-synchronous orbit (SSO) satellite, which passes through the perihelion of its orbit at the same local time, is useful for imaging, intelligence, and weather satellites [7].

For the development of reliable LEO satellite links, it is crucial to predict the electromagnetic (EM) wave propagation in highly variable atmospheric environments which can significantly deteriorate the performance of communication systems. In general, EM waves propagate through the atmosphere while experiencing refraction, reflection, and retardation. In particular, the troposphere, stratosphere, and ionosphere are the main areas in which atmospheric effects

The associate editor coordinating the review of this manuscript and approving it for publication was Giorgio Montisci.

take place. Both the tropospheric and stratospheric effects are caused by the spectral absorption of oxygen and water vapor molecules, though, meteorological phenomena occur only in the troposphere [8]. The spectral absorption of oxygen and water vapor molecule is considered as complex refractive index calculated by millimeter-propagation-model 93 (MPM93) [9]. Thus, such atmospheric environments can be quantified by measurements from meteorological observatories and transformed into an effective refractive index for the subsequent EM analysis. As such, one can study how atmospheric effects, such as attenuation, boresight error, and time delay, vary with the elevation angle and distance between satellites and ground stations. The attenuation and time delay are important in satellite link margin and distance measurements. The boresight error is an indicator that allows the beam to arrive the observation point by adjusting the antenna steering angle when the tracking area is fixed on the ground.

On the other hand, in the ionosphere being an anisotropic cold/magnetized plasma in the range of 60 to 1000 km above sea level, the atmospheric effects primarily depend on the extent of ionization and geomagnetic fields [10]. In order to consider the ionosphere effects on the EM propagation, the refractive index of the ionosphere is calculated by Appleton-Hartree equation [11]. The ionospheric effects are frequency dependent and can be neglected when operating frequencies are larger than 10 GHz.

There have been a number of previous studies that estimated atmospheric effects to the EM wave propagation in a phenomenological sense [12]–[16]. For example, the attenuation induced by water vapor was estimated for slant paths [12], the oxygen attenuation model was developed by taking the advantage of an extensive set of high-resolution radiosonde observations (RAOBS) collected in several sites worldwide [13], the geometric positioning method was suggested to the atmospheric refraction calibration for optical remote sensing satellite [14], and the experimental transmittance data were presented from urban and rural environments in the troposphere [15]. In addition, the EM wave propagation in the ionosphere modeled by anisotropic magnetized plasmas was numerically analyzed by using finite-difference time-domain (FDTD) with perfectly matched layers [16].

However, to our knowledge, theoretical analyses for the EM wave propagation from a LEO satellite to a ground station are still lacking. In our previous work, we have shown a new approach to analyze the EM wave propagation in a well-defined single radio link, which is from a geostationary orbit (GEO) to a ground station, using high frequency approximation such as geometric optics (GO), ray tracing technique, and physical optics (PO) [17]. Unlike GEO satellites, LEO satellites orbit Earth much faster, approximately more than 12 times a day, such that the radio links can be significantly affected by atmospheric effects. Therefore, one needs to collect meteorological data over a quite larger area to capture correct atmospheric effects.

In this paper, we propose a novel method to calculate the EM wave propagation from LEO to a ground station based on the PO, ray tracing technique, and GO considering interpolated atmospheric environments. Tropospheric and stratospheric environments are modeled by using meteorological data—air pressure and temperature, relative humidity, and rain rate—which are measured at 9 different radiosonde observatories in and around South Korea. Furthermore, we utilize piecewise cubic Hermite interpolating polynomial (PCHIP) and Kriging-exponential methods for vertical and horizontal interpolations of the raw meteorological data, respectively; interpolated atmospheric environments are amenable to the best use of ray tracing technique and GO. Subsequently, effective refractive indices of the stratified media can be extracted via MPM93. The ionospheric environment is characterized by the simplified Appleton-Hartree equation. Considering a sun-synchronous orbit satellite passing through South Korea, we calculate and discuss rain attenuation, atmospheric attenuation, boresight error, and received power for various conditions. Also, steering angle of the satellite antenna is calculated using boresight error and our analysis procedure so that the maximum received power is maintained at the observation point. To check the validity of the present method, our rain attenuation calculation results are compared with ITU-R. P. 618 model, physical model based on the rain-cell concept, and rain attenuation model in tropical regions [18]–[20].

II. ATMOSPHERIC ENVIRONMENTS

Meteorological data—air pressure and temperature, relative humidity, and rain rate—were measured at 9 different radiosonde observatories in and around South Korea, as shown in Fig. 1. A list of the radiosonde observatories and their geographic coordinates are provided in Table 1. 9 different radiosondes measured meteorological data from their observatories' altitudes (provided in Table 1) up to 30 km above the sea level with different vertical intervals. Therefore, aggregate meteorological data do not have an altitude match in general, as illustrated in Fig. 2. The vertical profiles of two sets of meteorological data measured at different observatories have no altitude matching. Moreover, horizontal locations of the observatories are highly irregular. Consequently, the raw meteorological data collected from all observatories may not be compatible with the use of the ray tracing technique and GO.

To solve this, the raw meteorological data are PCHIP-interpolated along altitude first. The resulting interpolated atmosphere consists of stratified layers with a fixed interval H_0, as depicted in Fig. 2. The use of PCHIP, which defines an interpolating function by means of polynomial pieces, ensures that some regularity conditions hold at the breakpoint [21].

Figs. 3-5 illustrate results of interpolated air pressure, air temperature, and relative humidity at 240 m above sea level by inverse distance weighting (IDW) and Kriging-exponential interpolation, respectively. The IDW

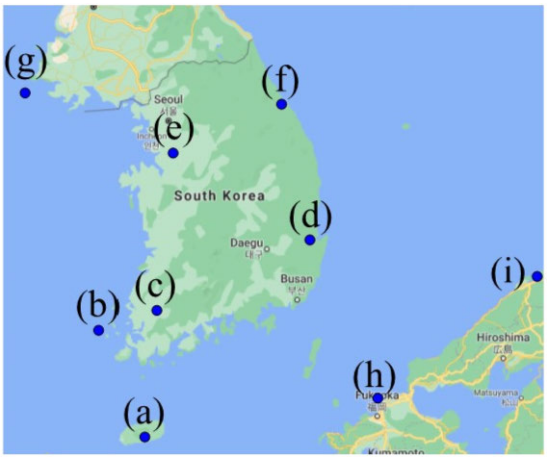

FIGURE 1. Horizontal locations of radiosonde observatories listed in Table 1.

TABLE 1. List of radiosonde observatories and their geographic coordinates.

Station	Latitude [degs, North]	Longitude [degs, East]	Altitude [m]
(a) National typhoon center	33.3315	126.6784	246.3
(b) Heuksando	34.6872	125.451	76.49
(c) Gwangju	35.1167	126.8167	13
(d) Pohang	36.0326	129.3796	2.28
(e) Osan	37.1	127.0333	52
(f) Bukgangneung	37.8046	128.8554	78.9
(g) Baeknyeongdo	37.974	124.7124	36
(h) Fukuoka	35.583	130.3833	15
(i) Matsue	35.458	133.0667	22

and Kriging-exponential interpolation method is applied to the PCHIP-interpolated meteorological data for the horizontal interpolation. We determined that the weighting of IDW is inversely proportional to the 1st power of the distance. We also approximated the semivariogram of the Kriging interpolation as an exponential function. The disadvantage of IDW interpolation is that it is sensitive to outliers and sampling configuration. Note that we adopt the Kriging-exponential model which has shown the highest accuracy against IDW, Gaussian and spline models in temperature interpolation from finite interpolation sites [22].

Fig. 6 illustrates the refractivity, denoted by N, which was obtained after applying MPM93 to the interpolated

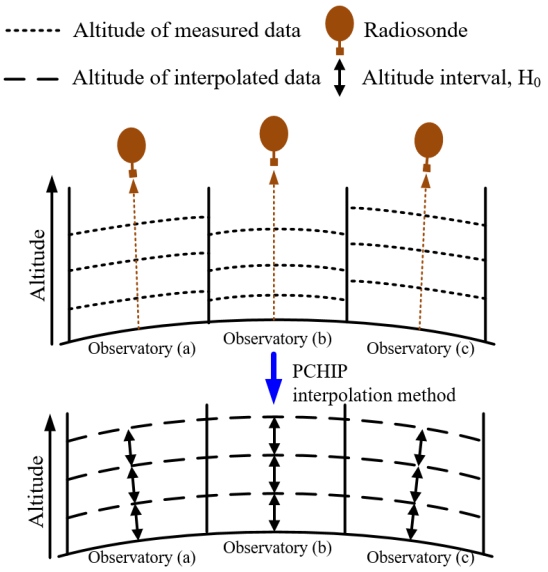

FIGURE 2. Altitude matching of the meteorological data measured at different observatories using PCHIP.

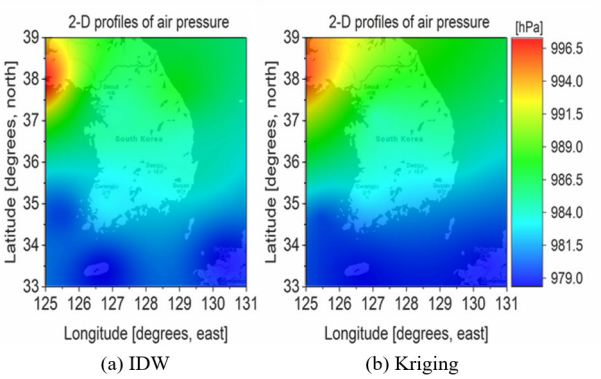

FIGURE 3. Interpolated air pressure (South Korea, 09:00, Sep. 06. 2020, 240 m above sea level).

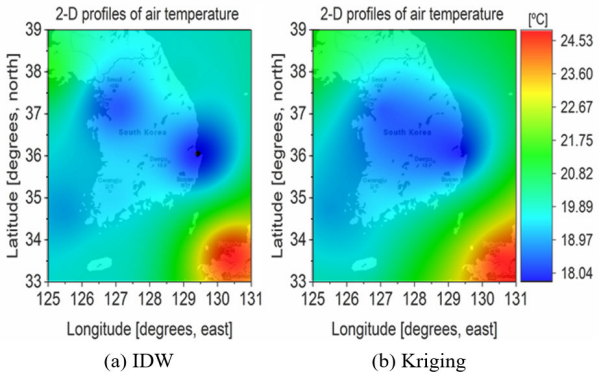

FIGURE 4. Interpolated air temperature (South Korea, 09:00, Sep. 06. 2020, 240 m above sea level).

meteorological data. The MPM93 calculates the complex refractivity N for given atmospheric conditions, such as air pressure, air temperature, and relative humidity.

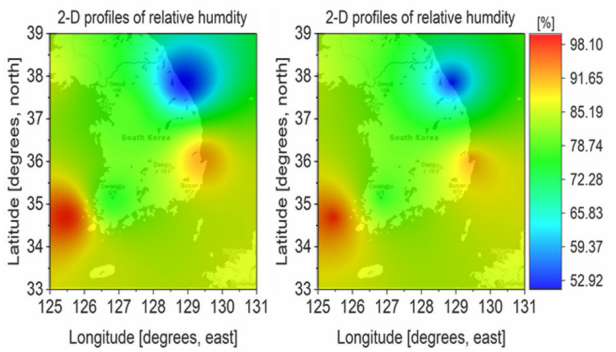

FIGURE 5. Interpolated relative humidity (South Korea, 09:00, Sep. 06. 2020, 240 m above sea level).

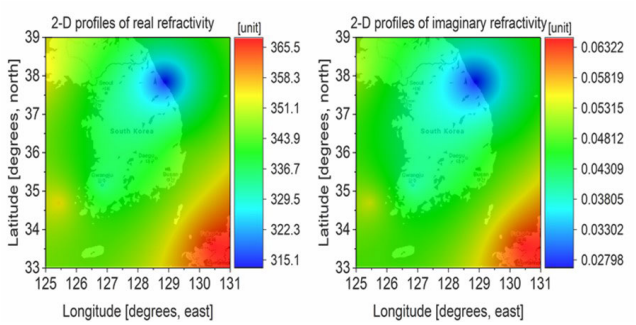

FIGURE 6. Interpolated complex refractivity (South Korea, 09:00, Sep. 06. 2020, 240 m above sea level, 35.75 GHz).

TABLE 2. Pearson's correlation coefficient between refractivity and meteorological data.

	Air pressure	Air temperature	Relative humidity
Real refractivity	-0.4035	0.7235	0.7036
Imaginary refractivity	-0.4760	0.7549	0.6924

Table 2 shows the Pearson's correlation coefficient between refractivity and meteorological data. The Pearson's correlation coefficient is calculated from the standard deviation of data X, σ_X, the standard deviation of data Y, σ_Y, and the expected value of X, Y and XY via (1). Each calculation is based on the data interpolated at 0.1 latitude and longitude intervals. The two-dimensional profiles of the refractivity are the most correlated with the air temperature of meteorological data. The correlation coefficient between real refractivity and imaginary refractivity is 0.9949.

$$\rho_{X,Y} = \frac{E(XY) - E(X)E(Y)}{\sigma_X \sigma_Y} \tag{1}$$

An effective refractive index n_{eff} in the troposphere and stratosphere can be calculated from the complex refractivity N via (2) where N' and N'' are real and imaginary values of N [17]. In the ionosphere (i.e., cold/magnetized plasmas), the effective refractive index can be calculated by

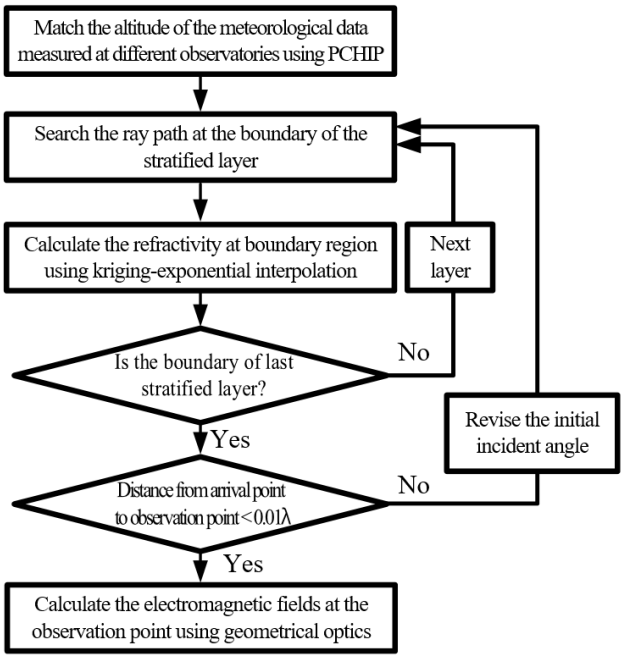

FIGURE 7. Overall analysis procedure of the EM wave propagation.

using Appleton-Hartree equation. Appleton-Hartree equation can be simplified to (3) because our target frequency is 35.75 GHz, where the Earth's magnetic field and electron collision are negligible when the electron density is at a typical concentration. The effective refractive index n_{eff} in the ionosphere is calculated from electron density N_e, electron charge e, electron mass m, permittivity of free space, and angular frequency ω. Then, propagation constant γ and the effective intrinsic impedance η_{eff} can be calculated by (4) and (5) [17].

$$n_{eff} = 1 + N \times 10^{-6} = 1 + (N' + jN'') \times 10^{-6} \tag{2}$$

$$n_{eff,ionosphere} = \sqrt{1 - (\frac{\omega_p}{\omega_0})^2} = \sqrt{1 - \frac{N_e e^2}{\varepsilon_0 m \omega^2}} \tag{3}$$

$$\gamma = \alpha + j\beta = j\omega\sqrt{\mu_0 \varepsilon_0}(n' - jn'') \tag{4}$$

$$\eta_{eff} = \eta_0 \frac{1}{n' - jn''} \tag{5}$$

Fig. 7 depicts the overall analysis procedure to predict wave propagation in the atmosphere. PCHIP and Kriging-exponential interpolation methods, ray tracing technique, and GO are used to calculate the EM wave propagation between LEO satellite and ground station. We first stratify the atmosphere into more than 100 layers at regular intervals and utilize the PCHIP interpolation methods to have the raw meteorological data matched to regular altitude intervals. Then, the ray is shot with the initial angle of incidence from LEO satellite to the ground station. When the ray encounters the boundary of the stratified layer in the atmosphere, the transmission path is calculated from the difference of refractive index using ray tracing technique.

The effective refractive index in the stratified layer is calculated from the interpolated meteorological data using MPM93 and simplified Appleton-Hartree equation. The horizontal interpolation of the meteorological data is conducted using Kriging-exponential method whenever a ray reaches to boundary of stratified layer to consider the horizontal variations in reflexivity in the ray-tracing phase. The ray path and refractive index calculations are repeated until the ray arrives the last stratified layer. Then distance difference is evaluated between arrival point and observation point. The process of searching for the ray path is repeated by changing the angle of incidence until the distance error is less than 0.01 wavelengths. The angle of incidence is expressed in zenith angle and azimuth angle. Every iteration decreases the maximum error halved, making the rapid convergence of the zenith and azimuth angles. One can refer to [17] for more details about the ray tracing technique applied here.

If the ray path is fixed, the EM field is calculated at the boundary of the stratified layer. The reflection and transmission of the EM wave at an oblique angle upon a dielectric-dielectric interface is calculated by considering the polarization, direction, normal vector of the tangent plane at the boundary [23]. Incident EM fields at the boundary are calculated from transmitted EM fields using GO. Atmospheric effects such as attenuation, boresight error, and dispersion can be calculated from the EM field at the observation point.

III. CALCULATION RESULT

We calculate the atmospheric attenuation and refraction of the EM wave between LEO satellite and ground station using ray tracing technique, GO, and interpolation. The accuracy of the proposed method is validated by comparing our rain attenuation calculation with the rain attenuation of ITU-R. P. 618-13 model, physical model based on the rain-cell concept, and rain attenuation model in tropical region, as shown in Figs. 8 and 9 [18]–[20]. Time percentage is defined as a cumulative distribution of descending data. In our method and physical model based on the rain-cell concept, rain attenuation is calculated from rain rate instead of time percentage. Also, the algorithm of our method uses the refractive indices calculated from rain rates using MPM93. Therefore, the rain rates are calculated by applying time percentage to the model in ITU-R. P. 837-7 [25]. The time percentages of 5, 1, 0.5, 0.1, 0.05, 0.01, and 0.005% correspond to the rain rates 0.187, 3.819, 7.201, 20.236, 29.276, 61.419, 81.479 mm/h, respectively in South Korea. We used a fixed rain height, and the atmosphere was stratified into 200-meters-intervals.

The atmospheric effects, including atmospheric attenuation, excess atmospheric path length, dispersive effects, and boresight error, calculated by the proposed method and ITU-R. P.676-12 are shown in Table 3 [26]. Note that the proposed method can consider the boresight error through the EM analysis whereas ITU-R. P.676-12 cannot.

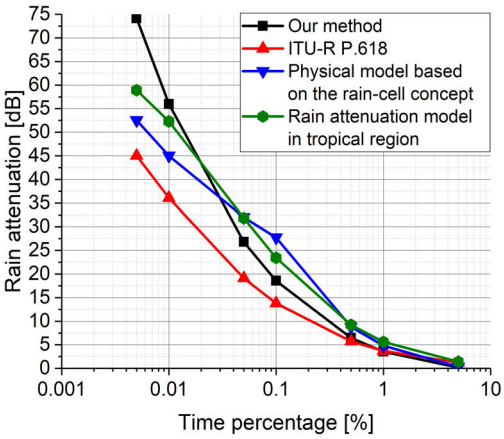

FIGURE 8. Comparison of rain attenuation calculated by our method, ITU-R. P. 618, physical model (rain cell), and rain attenuation model (tropical region) by time percentage (elevation angle: 60 degrees, 35.75 GHz, rain height: 3.601 km [24]).

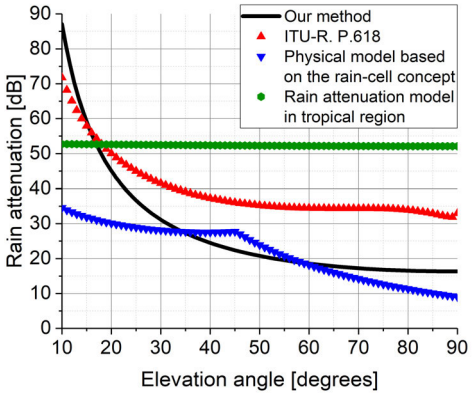

FIGURE 9. Comparison of rain attenuation calculated by our method, ITU-R. P. 618, physical model (rain cell), and rain attenuation model (tropical region) by elevation angle (35.75 GHz, rain rate: 20.236 mm/h rain height: 3.601 km [24]).

TABLE 3. The comparison of atmospheric effects calculated by our method and ITU-R. P.676-12 at 35.75 GHz for elevation angles of 30° one-way traversal (South Korea, Sep. 06. 2020, point source).

	Atmospheric attenuation [dB]	Excess atmospheric path length [km]	Dispersive effects [degs]	Boresight error [degs]
ITU-R. 676-12	0.832	0.000541	0.004674	-
Our method	1.227	0.033006	0.004652	0.0326

Consider the path of the SSO satellite, as described in Fig. 10. The SSO satellite passes through points A, B, C, and D over time. The altitude of orbit is 567.033 km above sea level, the inclination is 97.65754, and the period of orbit is 1.6 hours. The observation point is located at 240 m above sea level, 37.283 degrees north and 127.043 degrees east, equal to the latitude and longitude of point D. The location of point A was determined to have an elevation angle of 10 degrees and a coverage area of 1.76% [27].

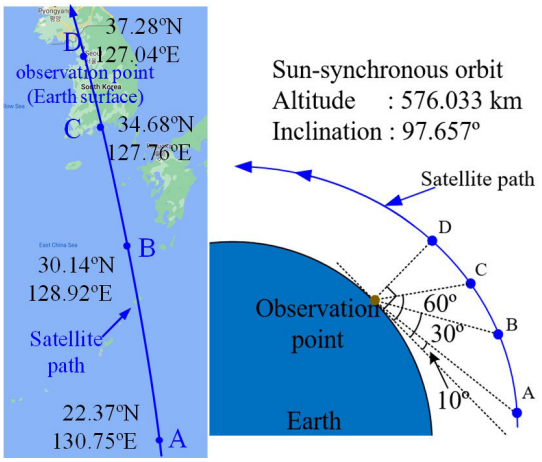

FIGURE 10. The path of the SSO satellite.

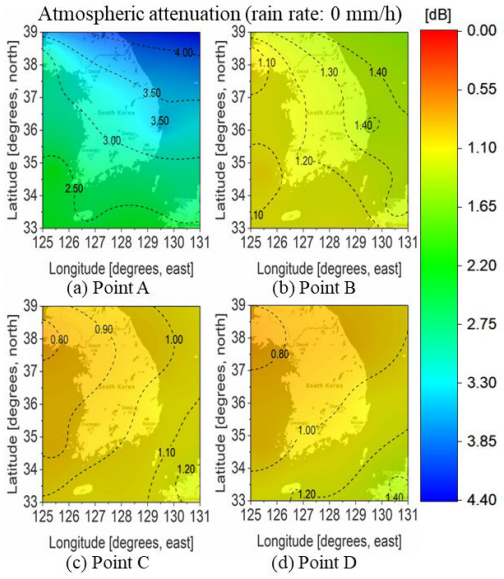

FIGURE 11. Atmospheric attenuation from LEO satellite to South Korea by satellite locations (Sep. 06. 2020, 09:00 AM, no rain).

Figs. 11(a)-11(d) illustrate the atmospheric attenuation from LEO satellite locations A, B, C and D to the ground station in the absence of rain by latitude and longitude, respectively. Atmospheric attenuation corresponds to the power difference between the received EM fields in the vacuum and the presence of atmospheric environments. The atmospheric attenuations for the satellite points A, B, C, and D are 3.274 dB, 1.218 dB, 0.876 dB, and 0.835 dB, respectively. In general, the atmospheric attenuation from LEO satellite to ground stations decreases as the satellite's location is closer to the observation point, though, the decreasing extent depends on the distribution of the refractive index in the atmosphere.

Figs. 12(a)-12(d) illustrate the atmospheric attenuation from LEO satellite to ground station when it rains uniformly with a rain rate of 7.201 mm/h in the atmosphere

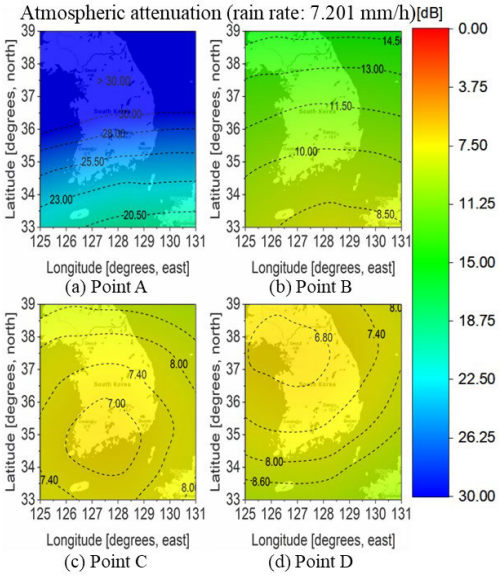

FIGURE 12. Atmospheric attenuation from LEO satellite to South Korea by satellite locations (Sep. 06. 2020, 09:00 AM, rain rate: 7.201 mm/h).

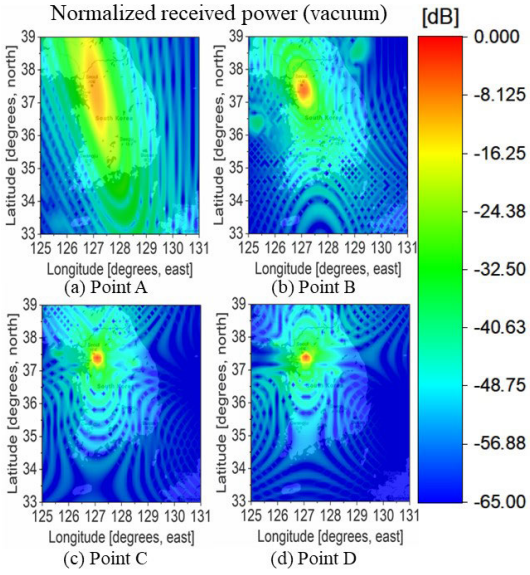

FIGURE 13. Normalized received power from LEO satellite to South Korea (Sep. 06. 2020, 09:00 AM, vacuum).

below 3.601 km by latitude and longitude. The atmospheric attenuations for the satellite points A, B, C, and D are 31.185 dB, 11.152 dB, 6.646 dB, and 5.842 dB, respectively. As the rain attenuation, which increases as the path length increases, dominates total attenuation, atmospheric attenuation decreases as the satellite gets closer to the observation point.

Figs. 13-15 show the normalized received power by latitude and longitude from LEO satellite to South Korea. The radiation of the parabolic reflector antenna is calculated using the PO on a reflector surface which is divided by less than

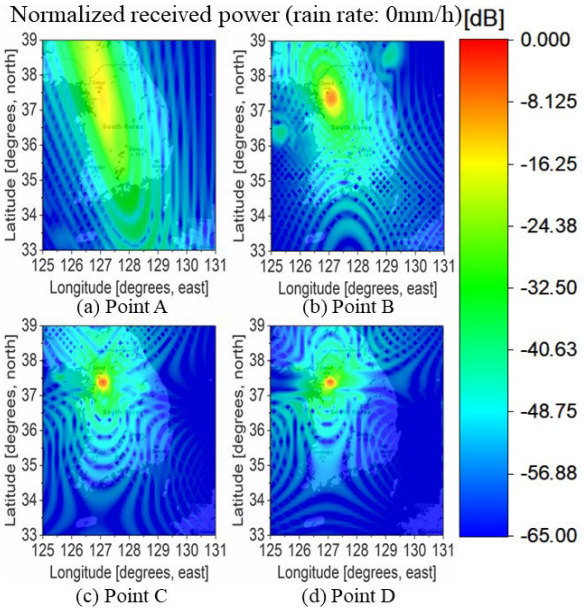

FIGURE 14. Normalized received power from LEO satellite to South Korea (Sep. 06. 2020, 09:00 AM, no rain).

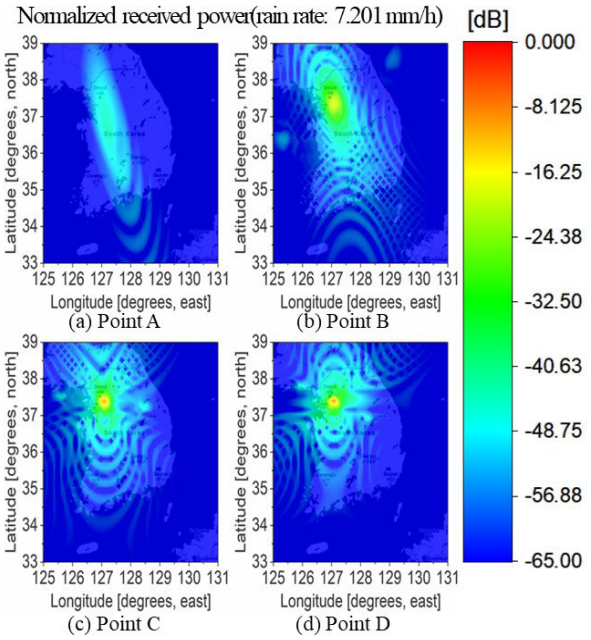

FIGURE 15. Normalized received power from LEO satellite to South Korea (Sep. 06. 2020, 09:00 AM, rain rate: 7.201 mm/h).

1/10 wavelength. The parabolic reflector antenna's size and focal length are the same as those of the CubeSat reflector antenna developed by the national aeronautics and space administration (NASA) jet propulsion laboratory (JPL) [28]. We assume that as the satellite moves the main lobe is adapted to the direction toward the observation point (the latitude of 37.283 degrees north and longitude of 127.043 degrees, east). In the absence of the atmosphere (viz., vacuum), the normalized received power is shown in Fig. 13(a)-13(d). Each normalized received power is calculated by the ratio of the received power to the maximum received power when the satellite is located at point D. Note that we account for the antenna's gain and elevation angle in the calculation of the received power. It is interesting to observe in Figs. 13(a), 13(b), 13(c), and 13(d) that the observation point and location for which the received power becomes maximized do not coincide even though the antenna is directing toward the observation point. The separation distance for the satellite points A, B, C, and D was recorded 8211 m, 456.8 m, 45.4 m, and 0 m, respectively. When the antenna's gain or elevation angle become higher, the separation distance gets smaller.

In the atmosphere without rain, the normalized received power from LEO satellite to South Korea is illustrated by latitude and longitude in Figs. 14(a)-14(d). With the decrease of the elevation angle, the boresight error increases, and the maximum received power decrease. The boresight error refers to the angular difference between the direct path and the path in the atmosphere, from the satellite to the observation point for the maximum received power.

In the atmosphere with a rainfall of 7.201 mm/h, the normalized received power from LEO satellite to South Korea is illustrated by latitude and longitude in Figs. 15(a)-15(d). Compared with Fig. 14, the boresight error increases, and the maximum received power decreases due to rainfall in general. Table 4 lists atmospheric effects and compensation angle from LEO satellite to observation point shown in Fig. 14 and 15. The received power and location of maximum received power depend on the satellite location and rain rate. Atmospheric attenuation can be indirectly evaluated by taking the power difference between the maximum received powers in vacuum and each atmospheric environment. In Fig. 14(a)-14(d), the power difference is 14.84 dB, 6.75 dB, 2.09 dB, 0.83 dB, respectively. And in Fig. 15(a)-15(d), the power difference under rainfall is 48.62 dB, 17.74 dB, 8.44 dB, 6.33 dB, respectively. In all four cases, the power difference is larger than atmospheric attenuation evaluated in Figs. 11 and 12. In Figs. 11 and 12, we calculated the atmospheric attenuation assuming that the antenna is a complex point source which generates a single ray with the perfectly coherent phase characteristics. On the other hand, the reflector antenna, modeled by many complex point sources distributing over the reflector surface, creates a bundle of rays having a pseudo-random phase front. This leads to the power weakening of a main beam due to inhomogeneous atmospheric environments in each ray's path. The boresight error and power difference decrease as the satellite moves from point A to point D over time. The steering angle of the antenna is compensated by using the boresight error and repeating our analysis procedure until the maximum received power approaches the observation point sufficiently. In all case except for Fig. 15(d), the maximum received power approached sufficiently to observation point within 2 iterations.

TABLE 4. The comparison of atmospheric effects from LEO satellite to observation point (Sep. 06. 2020, 09:00 AM, 45.45 dBi reflector).

Satellite location (atmospheric environment)	Location of maximum received power [degs]	Power difference [dB]	Boresight error [degs]	compensation angle [degs]
A, Fig. 13(a) (vacuum)	37.2078 N 127.0574 E	10.28	0.0500	0.0505
B, Fig. 13(b) (vacuum)	37.2794 N 127.0434 E	5.11	0.0116	0.0116
C, Fig. 13(c) (vacuum)	37.2826 N 127.0433 E	1.13	0.0040	0.0040
D, Fig. 13(d) (vacuum)	37.283 N 127.043 E	-	0	0
A, Fig. 14(a) (0 mm/h)	37.1388 N 127.0654E	14.67	0.1026	0.1066
B, Fig. 14(b) (0 mm/h)	37.2784 N 127.0435 E	6.74	0.0148	0.0148
C, Fig. 14(c) (0 mm/h)	37.2825 N 127.0433 E	2.09	0.0048	0.0048
D, Fig. 14(d) (0 mm/h)	37.283 N 127.043 E	0.83	0	0
A, Fig. 15(a) (7.201 mm/h)	36.711 N 127.1251 E	44.01	0.4327	0.6017
B, Fig. 15(b) (7.201 mm/h)	37.2725 N 127.0442 E	17.71	0.0339	0.0341
C, Fig. 15(c) (7.201 mm/h)	37.2822 N 127.0436 E	8.44	0.0081	0.0081
D, Fig. 15(d) (7.201 mm/h)	37.283 N 127.043 E	6.33	0	0

IV. CONCLUSION

A novel method to calculate the EM wave propagation from LEO satellite to ground station has been proposed. PO, Ray tracing technique, GO, and interpolation methods were used to consider inhomogeneous atmospheric environments. In the troposphere and stratosphere, the meteorological data are measured at 9 observatories in and around South Korea to calculate the refractive index of the atmosphere. PCHIP and Kriging-exponential interpolation methods were used to tailor the highly irregular meteorological data into the preferrable form of using ray tracing technique and geometric optics. The ionospheric environment was characterized by the simplified Appleton-Hartree equation. We validated the proposed method for the rain attenuation calculation compared with previous rain attenuation models. In addition, we calculated the atmospheric attenuation, boresight error, received power and confirmed that atmospheric effects strongly depend on the satellite location and rain rate. Atmospheric effects such as boresight errors and atmospheric attenuation tend to decrease as the satellite's position is closer to the observation point. The steering angle of satellite antenna can be compensated by using the boresight error and our analysis procedure so that the maximum received power is maintained at the observation point. Also, when it rains, the attenuation increases further and the position of the maximum received power shifts more. Our method is useful for satellite mission such as navigation, surveillance, and constellation networks that require the accurate estimation of the satellite links from LEO satellite to the ground station.

REFERENCES

[1] E. Buchen, "Small satellite market observations," in *Proc. 29th Annu. AIAA/USU Conf. Samll Satell.*, Atlanta, GA, USA, 2015, pp. 1–12.
[2] I. Fajardo, A. A. Lidtke, and S. A. Bendoukha, "Design, implementation, and operation of a small satellite mission to explore the space weather effects in LEO," *Aerospace*, vol. 6, no. 10, p. 108, Sep. 2019.
[3] S. P. Neeck, T. J. Magner, and G. E. Paules, "Nasa's small satellite missions for earth observation," *Acta Astronautica*, vol. 56, pp. 187–192, Jan. 2005.
[4] D. N. Baker and S. P. Worden, "The large benefits of small-satellite missions," *Eos, Trans. Amer. Geophys. Union*, vol. 89, no. 33, pp. 301–302, Aug. 2008.
[5] Z. Qu, G. Zhang, H. Cao, and J. Xie, "LEO satellite constellation for Internet of Things," *IEEE Access*, vol. 5, pp. 18391–18401, Sep. 2017.
[6] C. S. Ruf, C. Chew, T. Lang, M. G. Morris, K. Nave, A. Ridley, and R. Balasubramaniam, "A new paradigm in earth environmental monitoring with the CYGNSS small satellite constellation," *Sci. Rep.*, vol. 8, no. 1, pp. 1–13, Jun. 2018.
[7] D. A. Vallado, *Fundamentals of Astrodynamics and Applications*, 2nd ed. El Segundo, CA, USA: Microcosm Press, 2001.
[8] H. J. Liebe, "MPM—An atmospheric millimeter-wave propagation model," *Int. J. Infr. Millim. Waves*, vol. 10, no. 6, pp. 631–650, Jun. 1989.
[9] H. J. Liebe, "Propagation modeling of moist air and suspended water/ice particles below 1000 GHz," in *Proc. 52nd Spec. Meeting Electromagn. Wave Property Panel*, Palma, Spain, 1993, pp. 3-1–3-10.
[10] *Ionospheric Propagation Data and Prediction Methods Required for the Design of Satellite Services and Systems*, document Rec. ITU R-531, 2019.
[11] K. G. Budden, *Radio Waves in the Ionosphere*. Cambridge, U.K.: Cambridge Univ. Press, 2009.
[12] L. Luini, C. Riva, and L. Emiliani, "Attenuation induced by water vapor along earth-space links: Selecting the most appropriate prediction method," *IEEE Trans. Antennas Propag.*, vol. 65, no. 7, pp. 3806–3808, Jul. 2017.
[13] L. Luini and C. G. Riva, "A simplified model to predict oxygen attenuation on earth-space links," *IEEE Trans. Antennas Propag.*, vol. 65, no. 12, pp. 7217–7223, Dec. 2017.
[14] Y. Wang, Y. Zhu, M. Wang, S. Jin, and Q. Rao, "Atmospheric refraction calibration of geometric positioning for optical remote sensing satellite," *IEEE Geosci. Remote Sens. Lett.*, vol. 17, no. 12, pp. 2130–2134, Dec. 2020.
[15] S.-S. Oh, J.-W. Choi, D.-W. Kim, Y.-C. Lee, and B.-L. Cho, "Comparison of 0.75–24-GHz reach distances and ratios using propagation path loss measurements from urban and rural line-of-sight environments," *J. Electromagn. Eng. Sci.*, vol. 21, no. 1, pp. 1–7, Jan. 2021.
[16] J. Cho, M.-S. Park, and K.-Y. Jung, "Perfectly matched layer for accurate FDTD for anisotropic magnetized plasma," *J. Electromagn. Eng. Sci.*, vol. 20, no. 4, pp. 277–284, Oct. 2020.
[17] C. Kim, J. Heo, K.-Y. Jung, H. Choo, and Y. B. Park, "Propagation from geostationary orbit satellite to ground station considering dispersive and inhomogeneous atmospheric environments," *IEEE Access*, vol. 8, pp. 161542–161550, Sep. 2020.
[18] W.-G. Kang, T.-H. Kim, S.-W. Park, I.-Y. Lee, and J.-K. Pack, "Modeling of effective path-length based on rain cell statistics for total attenuation prediction in satellite link," *IEEE Commun. Lett.*, vol. 22, no. 12, pp. 2483–2486, Dec. 2018.
[19] J. X. Yeo, Y. H. Lee, and J. T. Ong, "Rain attenuation prediction model for satellite communications in tropical regions," *IEEE Trans. Antennas Propag.*, vol. 62, no. 11, pp. 5775–5781, Nov. 2014.
[20] *Propagation Data and Prediction Methods Required for the Design of Earth-Space Telecommunication Systems*, document Rec. ITU-R. P. 618-13, Dec. 2017.
[21] S. Cuomo, A. Galletti, G. Giunta, and L. Marcellino, "Piecewise Hermite interpolation via barycentric coordinates," *Ricerche Matematica*, vol. 64, no. 2, pp. 303–319, Jun. 2015.
[22] W. Cao, J. Hu, and X. Yu, "A study on temperature interpolation methods based on GIS," in *Proc. 17th Int. Conf. Geoinform.*, Aug. 2009, pp. 1–5.
[23] C. A. Balanis, *Advanced Engineering Electromagnetics*, 2nd ed. Hoboken, NJ, USA: Wiley, 2012.
[24] *Rain Height Model for Prediction Methods*, document Rec. ITU-R-839, 2013.
[25] *Characteristics of Precipitation for Propagation Modeling*, document Rec. ITU-R-837, 2017.
[26] *Attenuation By Atmospheric Gases and Related Effects*, document Rec. ITU-R 676-12, Aug. 2019.

[27] S. Cakaj, B. Kamo, A. Lala, and A. Rakipi, "The coverage analysis for low earth orbiting satellites at low elevation," *Int. J. Adv. Comput. Sci. Appl.*, vol. 5, no. 6, pp. 1–5, 2014.
[28] N. Chahat, R. E. Hodges, J. Sauder, M. Thomson, E. Peral, and Y. Rahmat-Samii, "CubeSat deployable Ka-band mesh reflector antenna development for earth science missions," *IEEE Trans. Antennas Propag.*, vol. 64, no. 6, pp. 2083–2093, Jun. 2016.

CHANGSEONG KIM (Student Member, IEEE) received the B.S. degree from the Department of Electrical and Computer Engineering, Ajou University, Suwon, Republic of Korea, in 2015, where he is currently pursuing the integrated M.S. and Ph.D. degrees with the Department of AI Convergence Network. His research interests include electromagnetic wave propagation and metasurface antenna.

DONG-YEOP NA (Member, IEEE) received the B.S. and M.S. degrees in electrical and computer engineering from Ajou University, Suwon, South Korea, in 2012 and 2014, respectively, and the Ph.D. degree in electrical and computer engineering from The Ohio State University, Columbus, OH, USA, in 2018. He is currently a Research Scientist with Purdue University. His research interests include computational electromagnetics, particle-in-cell, and quantum electromagnetics.

YONG BAE PARK (Senior Member, IEEE) received the B.S., M.S., and Ph.D. degrees in electrical engineering from the Korea Advanced Institute of Science and Technology, South Korea, in 1998, 2000, and 2003, respectively. From 2003 to 2006, he was with the Korea Telecom Laboratory, Seoul, South Korea. In 2006, he joined the School of Electrical and Computer Engineering, Ajou University, South Korea, where he is currently a Professor. His research interests include electromagnetic field analysis, high frequency methods, metamaterial antennas, radomes, and stealth technology.